

Contents lists available at [ScienceDirect](#)

Food and Bioproducts Processing

journal homepage: www.elsevier.com/locate/fbp

IChemE

On the design and simulation of an airlift loop bioreactor with microbubble generation by fluidic oscillation

William B. Zimmerman^{a,*}, Buddhika N. Hewakandamby^b, Václav Tesař^c,
H.C. Hemaka Bandulasena^a, Olumuyiwa A. Omotowa^a

^a Department of Chemical and Process Engineering, University of Sheffield, Sheffield S10 2TN, UK

^b Department of Chemical and Environmental Engineering, University Park, Nottingham NG7 2RD, UK

^c Institute of Thermomechanics of the Academy of Sciences of the Czech Republic v.v.i., 182 00 Prague, Czech Republic

A B S T R A C T

Microbubble generation by a novel fluidic oscillator driven approach is analyzed, with a view to identifying the key design elements and their differences from standard approaches to airlift loop bioreactor design. The microbubble generation mechanism has been shown to achieve high mass transfer rates by the decrease of the bubble diameter, by hydrodynamic stabilization that avoids coalescence increasing the bubble diameter, and by longer residence times offsetting slower convection. The fluidic oscillator approach also decreases the friction losses in pipe networks and in nozzles/diffusers due to boundary layer disruption, so there is actually an energetic consumption savings in using this approach over steady flow. These dual advantages make the microbubble generation approach a promising component of a novel airlift loop bioreactor whose design is presented here. The equipment, control system for flow and temperature, and the optimization of the nozzle bank for the gas distribution system are presented.

© 2009 The Institution of Chemical Engineers. Published by Elsevier B.V. All rights reserved.

Keywords: Airlift loop bioreactor; Microbubble generation; Fluidic oscillators; Transport phenomena; Biorefineries

1. Introduction

Airlift reactors are perceived to have performance advantages over bubble columns and stirred tank bioreactors for many applications, biorenewables production in particular. Where the product is a commodity biochemical or biofuel, energy efficiency is the primary concern. There are multiple objectives for the optimization of energy efficiency, however. The hydrodynamics of stirring is an important consideration, as are the phase transfer of nutrient influx and the efflux of inhibitor products and byproducts. Finally, the metabolism of cells or microbes engaged in the biochemical production are a major constraining factor – mass transfer from the bulk liquid to the bioculture must be maintained. There are two important reasons to use airlift loop bioreactors (ALB) that arise from the airlift effects: flotation and flocculation. Small bubbles attached to particles or droplets significantly lower the density of the aggregate. Grammatika and Zimmerman (2001) describe these generalized flotation effects. Such aggregates

are susceptible to floc formation. Typically, microbes or cells that sediment out of the suspension accumulate in stagnation zones at the bottom expire.

Given the importance of energy usage in the operation of ALBs, it is surprising that the sparging system, which is the central power consumption feature of the ALB, has not received more attention. Jones (2007) gives a good review of the major features of ALB, including the conventional types of sparger design. Chisti and Moo-Young (1987) classify the spargers used in the ALB as dynamic and static. Dynamic spargers use injection through nozzles to disperse the gas introduced. Static spargers are typically less reliant on the momentum of the jet, and the gas is introduced typically through a perforated plate (see Deshpande and Zimmerman, 2005a,b) or less commonly, through a porous baffle (Heijnen and Van't Tiet, 1984). This study was motivated by the development of a novel microbubble generation technique based on fluidic oscillation diverting jets used in sparging (Zimmerman et al., 2008).

* Corresponding author. Tel.: +44 114 222 7517; fax: +44 114 222 7501.

E-mail address: w.zimmerman@sheffield.ac.uk (W.B. Zimmerman).

Received 7 November 2008; Received in revised form 20 March 2009; Accepted 23 March 2009

The paper is organized as follows. In Section 2, the microbubble generation mechanism by fluidic oscillation is discussed, leading to design criteria for sparging systems and nozzle banks that achieve high energy efficiency. In Section 3, aspects of the design of ALBs that are influenced by the incorporation of the microbubble generator by fluidic oscillation, the design itself, and simulation of an such an ALB are presented. In Section 4, a summary is given and conclusions are drawn.

2. Microbubble generation

The concept for the fluidic oscillator driven microbubble generation mechanism (Zimmerman et al., 2008) stems from the systems biology objective of using oscillatory nutrient feed streams in a conventional fermentor or chemostat to investigate the kinetics of metabolic pathways. Zimmerman (2005) demonstrated from the simulation of the glycolytic pathway in yeast that oscillating the glucose feed stream could create information-rich time series responses in extracellular metabolic production, such as excreted ethanol. Specifically, it was shown that three kinetics coefficients of the Michaelis–Menten kinetics of the branch point of succinic acid production could be inferred by data assimilation with high fidelity due to the presence of strong nonlinearity excited at one of two resonant frequencies of the pathway. The eigen-system analysis of the pathway showed natural (but decaying) frequencies in the pathway at 15 Hz and 52 Hz. The latter was identified by eigenvector analysis as AMP-ATP, NAD-NADH co-metabolite oscillations. The former involved four reactions to which pyruvate was essential.

As such oscillations are not observable in unforced chemostats, in order to test the hypothesis, the first author sought an approach for designing a bioreactor which would have an easily controllable and oscillating nutrient stream. As liquid phase oscillation is difficult to achieve at low flowrates, the obvious stream to control would be pneumatic. Thus the introduction a gas stream with a nutrient in the gaseous phase would be ideal. The easiest nutrient to introduce for most biocultures is oxygen, so the target switched from yeast fermentation to processes controlled by aeration rate, an important example of which is wastewater treatment.

Purification, treatment, or removal of contaminants from water is often associated with their decomposition. An important method, the biological treatment of water, is essentially an intensification of the naturally occurring decomposition of contaminant by action of micro-organisms, mainly bacteria. Though this method alone cannot remove all possible contaminants (and especially for treatment of various industrial wastewaters has to be often combined with other methods) it is effective and commonly applied method for breaking down the major pollutants: organic matter, nitrates and phosphates (Stevenson, 1997). The efficiency of the process – or, more specifically of the aerobic stage of the biological decomposition – is limited by availability of oxygen needed for growth and activity of aerobic micro-organisms.

We proposed to combine a fluidic oscillator with a nozzle bank with the intention of producing an oscillatory stream of bubbles. Tesař et al. (2006) had previously developed a simple and inexpensive no-moving part fluidic device with adjustable frequency in the range of 1–100 Hz, controllable by changing the length of the feedback loop, but for essentially high Reynolds number flows achievable even a low air flow rates.

This range of frequencies includes the target range of the natural biochemical pathways oscillations of glycolysis in yeast, so are likely to be excited by bacterial cultures which exhibit glycolytic cycles in aerobic metabolism. However, it also occurred to us that there was the potential to generate microbubbles by a novel mechanism using fluidic oscillation. Typically, bubbles generated from a rigid aperture are approximately an order of magnitude larger than the aperture. Unfortunately, even using extremely small holes does not necessarily ensure generating small air bubbles. Bubbles grow during the process of their formation and when finally separated from the aperture exit, their diameter is often many times larger than the hole diameter. The separation is controlled by surface tension of the water; and an important negative factor is the fact that many contaminants – especially organic – present in wastewater are known to increase the surface tension. The final bubble size is commonly determined by the overcoming of the wetting force of the pre-bubble on the solid walls by buoyant forces or by currents in the liquid. The fluidic oscillation, if appropriately configured and tuned, could interfere with this balance of forces as the pre-bubble reaches sizes not much larger than the aperture diameter, since the acceleration force of the oscillation can be made arbitrarily large by using high frequencies and large amplitude oscillation from jet diversion. Such a microbubble generator would have the benefit of very little additional energy (pumping head loss) to break off the bubble, so should be highly energy efficient in formation.

In this section, we discuss the potential design benefits of microbubbles so produced and the methodologies of their production that we have engineered, primarily with the target of increasing the mass transfer for aeration in bioreactors, but the principle applies to just about any nutrient introducible in the gaseous phase.

2.1. The benefits of microbubbles

Why is that when blowing a continuous stream of air through a small opening that we do not typically get small bubbles? For instance, when a bubble is formed from a single opening, the liquid attached to its perimeter provides an anchoring effect as the wetting force attaches the growing bubble to the solid surface. Unless this anchoring force is disturbed, the bubble will grow until the buoyant force on the bubble exceeds the anchoring restraint on the bubble, causing it to pinch off. Typically, the buoyant force does not exceed that of the wetting anchor until the bubble is about an order of magnitude larger than the diameter of the hole. The process is sensitive to the wetting properties of the solid surface as well. If the bubble contacts the surface over a larger region than the aperture perimeter, or if the solid surface is hydrophobic, the gas phase of the growing bubble will form a second anchor force with the solid surface over a wider area, increasing the buoyant force and thus bubble volume required to overcome it. If the surface is hydrophilic, then this attractive force is absent. In the next subsection, the generation mechanism for microbubbles by fluidic oscillation is discussed. In this section, the desirability of small bubbles is discussed.

The major advantage of small bubbles is the surface area to volume ratio. Nearly all interfacial transport processes – heat, mass, momentum – are dependent on the surface area of the interface between the phases. It is geometrically clear that the surface area to volume ratio of a spherical bubble increases

inversely proportionate to its radius or diameter:

$$\frac{S}{V} = \frac{4\pi r^2}{(4/3)\pi r^3} = \frac{3}{r} \quad (1)$$

This may appear algebraically equivalent, but suppose we maintain that the total volume V_0 of the bubble phase is to remain constant, then

$$S = \frac{3}{r} V_0 \quad (2)$$

is the surface area that the total phase exhibits. For instance, if 1 l of air is distributed in 100 μm size bubbles, there are 10 m^2 of interfacial area, easily comparable or greater than a reasonable sized air–liquid interface of the continuous phases in a tank open to the atmosphere. Furthermore, the bubbles are moving. The mass transfer coefficient of a single bubble or droplet may be difficult to assess, as it depends on the hydrodynamics of bubble rise, its environment, and the constitutive properties of the medium and material transferred (see [Deshpande and Zimmerman, 2005a,b](#)), but in most flows it is dominated by convection forces and can be globally fitted to a mass transfer coefficient phenomenological equation, where the overall flux is proportional to the interfacial area S of the dispersed phase. Thus transfer dynamics, mass or, by analogy, heat flux, are rapidly enhanced by decreasing the bubble size. The above argument for the benefit in transfer efficiency is typified by the common chemical engineering phenomenological description of interphase mass transfer flux J (mol/s):

$$J = K_l S (c_g - c_l) \quad (3)$$

where K_l is the mass transfer coefficient (units of velocity), S is the interfacial area, and c_g and c_l are molar concentrations. Mass flux J , all things being equal, increases proportionate to S , and therefore inversely proportionate to the diameter d of the microbubble. [Bredwell and Worden \(1998\)](#) inferred K_l in an oxygen microbubble column from a plug flow concentration model for the dissolved oxygen. A laser diffraction technique was used to compute the interfacial area S . [Worden and Bredwell \(1998\)](#) demonstrate that the very high mass transfer rates of microbubbles require modeling of an intrinsically transient nature. They found that the presence of non-transferred gas in the microbubble limited the mass transfer rates.

But one might argue that this flux enhancement effect is balanced by the cost of producing microbubbles. As we pointed out in the beginning of this section, one would think that to produce smaller bubbles requires smaller holes or pores. Therefore, with continuous flow through these smaller openings, the friction force would be expected to be proportionately larger. As friction increases with surface area of pores or channels, one would expect the head loss on the pump due to hydraulic resistance to rise inversely proportionate to the opening diameter. So the transfer performance increase is offset by the energetic decrease, and no expected overall efficiency is likely. This argument, however, argues against seeking to produce smaller bubbles by miniaturizing the hole. The “win” can only occur if the friction loss remains about the same, but the bubble size is reduced. A different mechanism for bubble production is required. The next section discusses the fluidic oscillator driven microbubble formation mechanism reported by [Zimmerman et al. \(2008\)](#), and the following section reports its surprising decrease in friction loss against

the control of continuous flow through a pipework network and distributed diffuser aeration system in pilot trials.

As an aside, the argument given above for mass and heat transfer enhancement by smaller bubbles with equivalent volume of dispersed phase holds for momentum transport too, with some modification. The classical Stokes law serves as a guide for the residence time of a microbubble in a viscous liquid:

$$U_{\text{stokes}} = \frac{2}{9} \frac{g \Delta \rho d^2}{\mu_l} \quad (4)$$

Due to the square, it is clear that the residence times of small bubbles is markedly longer for the same height of liquid than for larger bubbles. Thus smaller bubbles have much longer to transfer their momentum from the bubble to the liquid dragged along with them, even though they have less momentum to transfer. These two effects would balance, but for the surface area to volume ratio – momentum is also transferred, by shear stress, across the surface area of the bubble. Therefore the flux of momentum is markedly increased by the decrease in bubble size, by the same ratio of Eq. (2). It follows that microbubbles have a higher “dragging ability” when rising or flotation capability with the same volume of fluid holdup. This effect is potentially very important for improved mixing in a riser region of an airlift loop bioreactor, provided the bubbles can be produced energetically efficiently, i.e. the cost of the microbubble production per unit volume does not rise due to rising friction factor. For design purposes, if the goal is to achieve the same mixing level or riser performance with microbubbles, then potentially this can be achieved by a lower volumetric flow rate, since the longer residence time in the height of liquid permits higher holdup at lower volumetric flow rates.

These benefits have been tested in laboratory and pilot scale experiments. [Shi \(2006\)](#) demonstrated 8-fold smaller bubbles with oscillatory flow than with the same volumetric flow rate steady flow through the same nozzle bank, measuring an 8-fold increase in dissolved oxygen transfer efficiency according to the standard ASCE test. In a recently completed pilot scale trial, [Zimmerman and co-workers \(internal report\)](#) have found 3-fold increase in aeration rates using the fastest frequency oscillation possible in their fluidic oscillator system over steady flow through the same flexible membrane diffuser array with the same volumetric flow rate ($\sim 2\text{m}^3/\text{h}$ per diffuser). They also recorded a decrease in power draw on the blower to achieve this flow rate of 13%, which will be discussed in Section 2.3.

2.2. Microbubble generation by fluidic oscillation

2.2.1. Instability of parallel percolation

The desirable aerator would produce simultaneously a large number of very small air bubbles. This would result in a large total air/water interface area and therefore high rate of oxygen transport into water across this interface. In the various attempts at reaching this sought after situation, the aerators have been made with a large number of parallel tiny apertures exiting air into water. Unfortunately, the desirable bubble formation has never been obtained – because of the fundamental instability property of the bubble growth mechanism. At the beginning of the bubble formation, the distribution of air flow into the apertures is stable. This, however, ceases to be once one of the growing bubbles surpasses the hemispherical limit

shape. Immediately, its further growth then becomes easier. The air entering into it meets a lower pressure difference Δp to overcome than in the other apertures. As a result, this particular bubble starts growing faster at the expense of the other bubbles, which may even completely cease to grow.

This is demonstrated in Fig. 1, which shows photographs taken when watching a steady air flow into an aerator positioned at the bottom of a shallow water-filled tank. The aerator – actually the same as in the other experiments described here – has the air exit apertures in the form of a row of 0.6 mm diameter parallel holes. Despite the air flow path being equally easy in all the holes, the bubbles are formed in only one of them. The exceptional case is chosen by mere chance – in the two photographs in Fig. 2 under nominally identical conditions, different orifice are seen to be active. In this aperture, the bubbles grow to sizes substantially larger – by more than a decimal order of magnitude – than the hole diameter. All the other orifices are inactive, no bubbles are formed in them.

This failure to obtain the desirable parallel formation of tiny bubbles is very fundamental – it is the very basic Young–Laplace law of surface tension σ that governs the bubble formation. According to it, the pressure difference Δp across the air/water surface is inversely proportional to the curvature radius R of the surface:

$$\Delta p = \frac{2\sigma}{R} \quad (5)$$

When a bubble is formed in a round orifice exit, its curvature radius is initially extremely large, but decreases fast. The pressure needed for the bubble growth increases. The critical situation is reached once the growing bubble attains the hemispherical shape. Thereafter, its radius R increases with increasing volume and, consequently, the pressure difference Δp decreases. All the air then enters into the particular bubble that first forms a bubble where it meets less opposition to flow. This makes its further growth easier. This instability is essentially the same mechanism as Saffman–Taylor viscous fingering (Zimmerman and Homsy, 1991).

2.2.2. Jet diversion fluidic oscillation

The key idea of the microbubble generation method as described by Zimmerman et al. (2008), is to limit the bubble growth time by the duration of the period of an oscillator that supplies air into the bubble-formation apertures – which may be nozzles, diffusers, porous baffles, perforated plates or microporous materials. The growth is terminated at the end of each oscillation half-period. The bubble is then removed from the aperture so that the growth of the next bubble has to start anew in the next period. No bubble can reach the large size typical for steady blowing.

The essential part of the aeration system is therefore a fluidic oscillator – preferably, due to the advantages of reliability, robustness, and low price, an oscillator of the no-moving-part type – one of the variety described, e.g., by Tesař (2007). Shown in Fig. 2 is an example of a particularly suitable fluidic flow-diverting oscillator design. Its main component is the fluidic amplifier (originally designed for another application) shown in the left part of Fig. 2. Details of its geometry and properties are described by Tesař et al. (2006). Steady air flow is supplied into the terminal S and its flow into one the two output terminals Y_1 and Y_2 is controlled by the control action applied to the control terminals X_1 and X_2 . The control action deflects the jet of the air issuing from the main nozzle, which is connected to S. The device is described as an amplifier because the

powerful output flow through the output terminals Y_1 or Y_2 is controlled by much weaker control flows input into the control terminals X_1 and X_2 . This particular amplifier is bistable – it uses the Coanda effect to remain in one of its two stable states when the control action is absent.

The oscillator is made from the amplifier by providing it with a feedback loop. There are several possible feedback alternatives even for this jet-diverter type of amplifiers (as discussed in Tesař, 2007). The feedback loop shown at the right-hand part of Fig. 2 is the particularly simple one, consisting of nothing more than just a tube of suitable (or, in Fig. 2, adjustable) length, connecting the two control terminals X_1 and X_2 . As shown in the right-hand part of Fig. 2, the jet issuing from the main nozzle attaches to either one of the two attachment walls due to the Coanda effect of jet attachment to a nearby wall and is thereby led into one of the two output terminals. Because of the change of direction due to the deflection, air flow trajectories inside the jet in the vicinity of the control nozzles are curved. This curvature creates a radial pressure gradient across the jet. In the situation shown in Fig. 2, this causes a decrease in pressure at the control port X_1 , which then draws air through the feedback loop from the opposite control terminal X_2 where the pressure is higher. It takes some time for the flow in the feedback loop tube to gain momentum, but when this happens, the control flow in X_1 suffices, because of the amplification effect, for switching the main jet from the terminal Y_1 and diverting it into to the other terminal Y_2 . As the device is symmetric, this jet switching is – after a delay needed for the feedback flow to gain momentum into the opposite direction – then reproduced in the opposite way, thus leading to a periodic switching process. Tesař et al. (2006) demonstrate that the frequency of the oscillation is controlled primarily by the length of the feedback loop and the supply flow rate. The acoustic regime of frequencies between 1 and 100 Hz could be readily achieved in a model consisting of the plate stacks shown in Fig. 2.

Tesař (2007) reviews, apart from this jet deflection type, many other alternative types of fluidic oscillators that may be used to drive ALBs. All of them when used in this application, are supplied with steady air flow and produce self-excited air flow oscillation. Essentially, the oscillation due to an intrinsic hydrodynamic instability caused by the presence of the feedback action – the change in the large output flow due to the return flow of a small fraction of the fluid into a location where it can act against the cause which generated the output effect. The principles underlying the fluidic oscillators can be classified into three groups:

- (1) Twin valve oscillators with mutual – phase shifted – blockage by fluidic amplifiers capable of producing the flow turn down effect. This is a rather rarely used principle.
- (2) An external feedback loop added to a single amplifier valve (or several valves forming an amplifying cascade). This is the very obvious and also very common operating principle, mostly used to generate an oscillatory or pulsatile fluid flow in a connected load with the jet-deflection amplifiers. Because of the symmetry of the amplifier, the oscillators usually possess two feedback channels, one connecting Y_1 with X_1 and the other connecting Y_2 with X_2 . It is the principle used here, having the less obvious single loop layout.
- (3) Internal feedback oscillator, sometimes using a geometry reminiscent of a fluidic valve, sometimes with rather

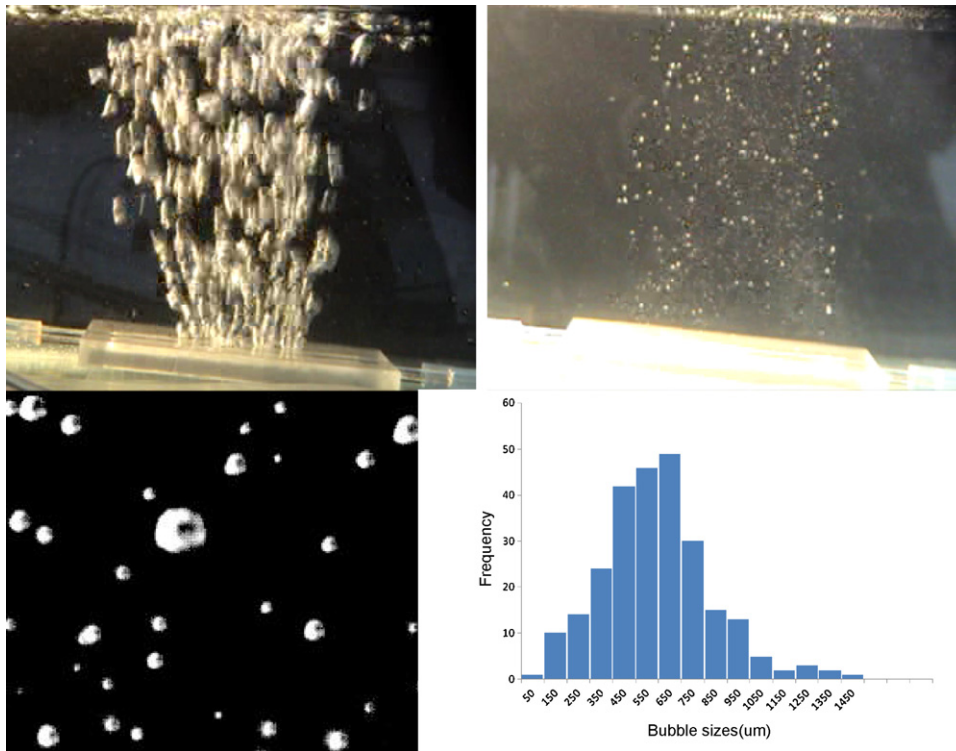


Fig. 1 – Examples of large bubble generation by steady blowing of air through small submerged orifices. The aerator is provided with an array of 600 μm parallel holes having their axes oriented vertically. Instead of the expected stream of many parallel small bubbles, the parallel percolation instability leads to generation of large bubbles – of size more than 10-fold larger (most bubbles on the top left are ~10 mm). The top right is an image from the same system but with the fluidic oscillator active. The flow rates are comparable but not equal, 2.5:1 in ratio. The steady flow does not have steady bubble production at the lower flow rate of the right hand image. At the higher flow rate of the steady flow, the oscillator induced bubbles are too closely spaced and coalesce. Eight images taken from the oscillator driven experiment in a 8.5 mm by 7.4 mm window were used to collect 237 bubble sizes (diameter of equivalent area circular section). It should be noted that the nozzle block is 12 cm long. The mean bubble size of the distribution of frequency is 700 ± 25 μm.

remote from it and perhaps retaining only topological similarity. Also used to generate an output fluid flow.

Any of these principles can be used to design an oscillator for generation of the oscillatory air flow for ALB. The

diverter configuration adopted here is particularly useful when employed for the flow diversion, as it can feed alternately one bank or the other of aerator nozzles, as these are shown in the schematic Fig. 3. The switching provides short pulses of momentum in the nozzles, which arrive with regular frequency at the exit apertures.

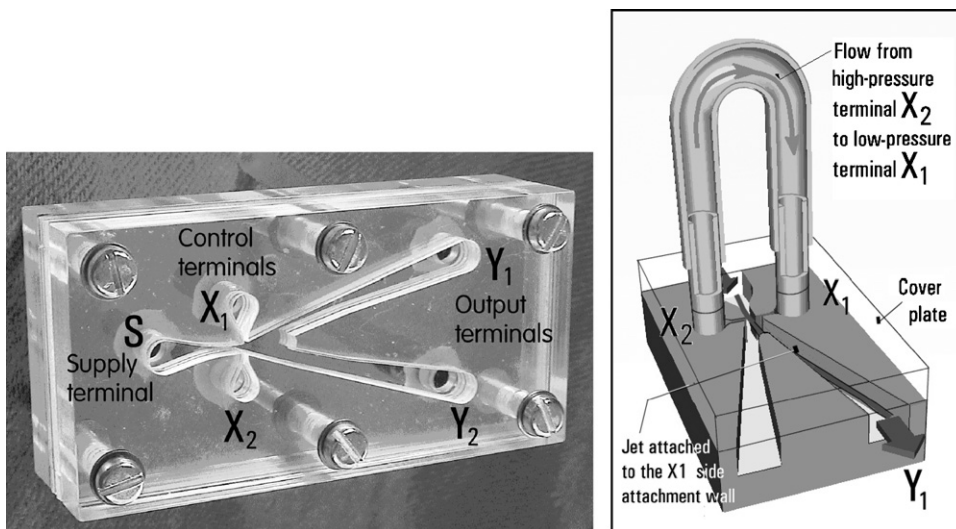


Fig. 2 – Left: the model of the fluidic jet-deflection amplifier used in the tests. It is a stack of PMMA plates with laser-cut cavities – containing no moving mechanical parts. The screws are 1/4 inch heads. Right: the fluidic oscillator is made from the amplifier by providing it with the feedback loop (shown here of adjustable length for tuning the oscillation frequency) connecting its two control terminals.

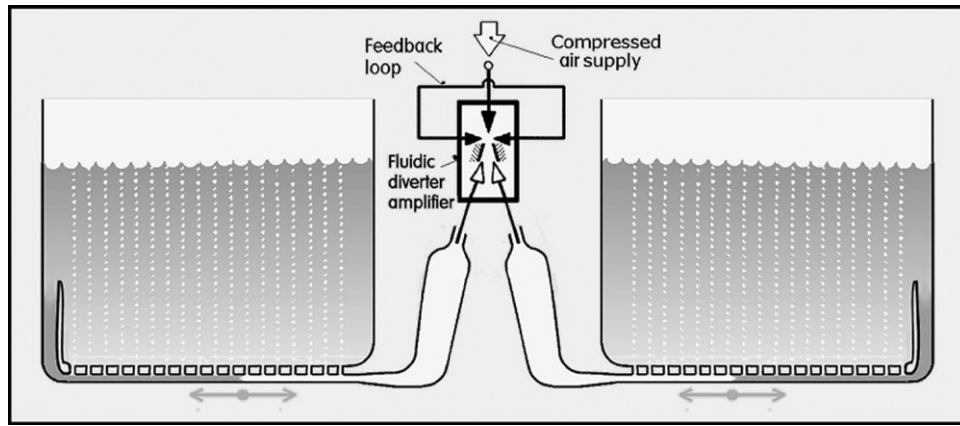


Fig. 3 – Schematic representation of the fluidic diverter oscillator driving the microbubble generation system with two nozzle banks fed by alternate oscillation “strokes”.

Applying the fluidic oscillator to the task of generation of the microbubbles rises is, however, not necessarily straightforward. The problem encountered is the removal of the nascent microbubble from its air inlet aperture while it is still smaller than the size of the critical, hemispherical cap.

Naturally grown bubbles separate from their apertures due to the hydrostatic lift force. This, however, reaches the necessary level only when the bubble is relatively very large. The small bubbles, not yet having reached the critical hemisphere shape, need not and often do not separate. When supplied with the oscillatory air flow, they may stay attached increasing and decreasing in size in the rhythm of the oscillation.

One possible solution is applying the oscillatory input air flow pulses with considerable momentum, sufficient to dislodge the nascent microbubbles. Adjusting the proper momentum is, however, rather difficult and experience shows it may need re-adjustments with changing operating conditions.

A rather less sensitive solution is the original concept of the authors to blow-off the nascent microbubbles by an adjacent water flow pulse in the other half of the oscillation period. In particular, this was demonstrated in a model presented in

Fig. 4. The water and air orifices are arranged in a grooved channel so that they form two rows, with their axes mutually at right angles. The bubbles that have grown during the first half of the oscillation period on the air side are blown off from their apertures in the second half of the period, during which the water flow pulse is admitted to the water side of the groove. Fig. 5 shows the success of this method, where the oscillatory flow generates microbubbles from the 600 μm holes of submillimetre size, whereas those generated by the steady flow are dominated by >6 mm bubbles. One observation from Fig. 5 (see bubble size distribution in Fig. 1) is that the small bubbles are approximately monodisperse and regularly spaced, and therefore do not suffer from coalescence. Crabtree and Bridgwater (1969) provide a mechanistic argument for the non-coalescence of chains of bubbles being hydrodynamically stabilized as they rise.

Additionally, another method of microbubble formation was demonstrated in a layout in which short small-diameter holes connect the exit orifice with a larger-diameter manifold. The aerator is supplied with the oscillatory flow delivered by the fluidic oscillator and operates in a periodic manner, during which alternating air and water columns move back and

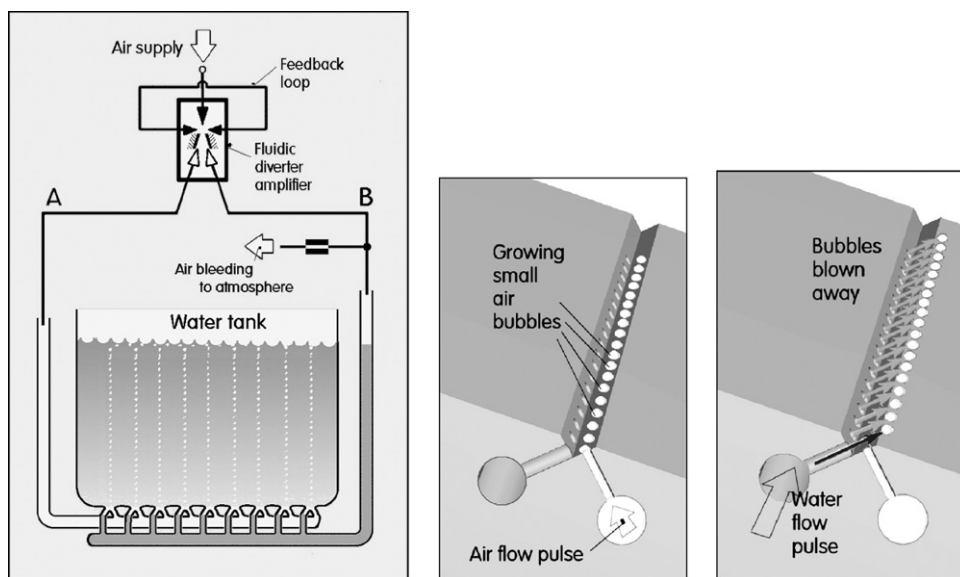


Fig. 4 – Left: configuration for the blow-off mechanism for bubble detachment. While the same diverter oscillator as in Fig. 3 is used, only one of its outputs, A, is used to deliver the air to the aeration apertures during the half-period. The other, B, delivers a water flow pulse into a system of adjacent water-flow nozzles. Centre: the bubble formation half of the period. Right: water flow pulse removes the nascent bubbles from their apertures.

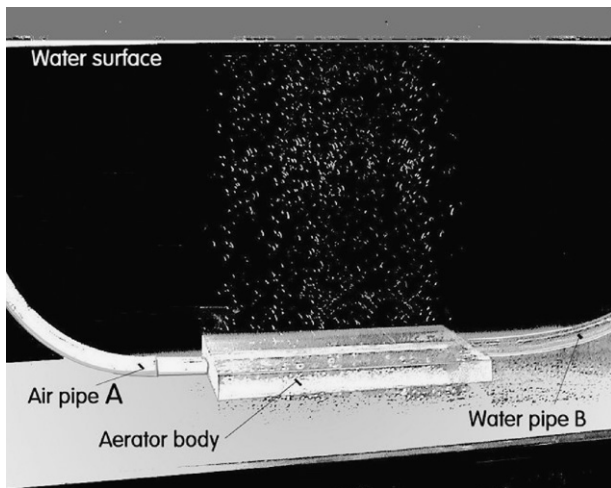


Fig. 5 – Tiny bubbles generated in an experiment with the aerator system model corresponding to Fig. 4. Actually, the same nozzle bank is used as the one generating the large bubbles with the steady (non-oscillated) air flow through the 0.6 mm holes as shown in Fig. 1.

forth through the manifold. During the first half of the period, the small holes are filled with air from an air column moving past them. In the following half-period, the liquid column comes and moves by. It enters the small holes and dislodges the air from them. This may seem to be a somewhat complex mechanism, but the formation of the alternating water and air columns in the manifold was observed to be automatic, new water columns forming and gradually progressing down the manifold as the air columns between them diminished, having lost their air by filling the small holes. An certain advantage of this method is the rather low required oscillation frequency, corresponding to the reciprocating motions of the liquid and air columns.

Although the “blow-off” configuration succeeds in creating small bubbles on the scale of the aperture, the price paid is that it uses half the momentum for air flow and bleeds off half the volumetric flowrate. It is a reasonable question to ask as to whether this price is essential. So the test of the same

configuration but without the water flow – air flow in both adjacent banks – was conducted, with the observation that small bubbles form from both banks of holes. Therefore, the essential feature is the orientation effect – a horizontal component is necessary. An artist’s conception of how horizontal orientation is necessary for only air flow is shown in Fig. 6.

The key element in this mechanism is the recoil of the nascent microbubble against the solid wall, and particularly the wetting properties of the microbubble. For instance, we fabricated nozzlebanks from microchannels wet etched in both glass and PDMS microchips. The glass microchips formed small bubbles of the size of the aperture with the microchannel apertures (60 μm characteristic size) oriented horizontally, but $\sim 500 \mu\text{m}$ bubbles when oriented vertically (Varma, 2007). The PDMS analogues only formed large bubbles. The bubble attaches to the PDMS surface and grows along the microchip exterior surface. As bubbles wet the PDMS surface but not the glass surface, it is clear that wetting properties of the orifice and adjacent solid wall are extremely important for the formation of microbubbles by the fluidic oscillation mechanism.

2.3. Energy efficiency

One of the unexpected outcomes of an ongoing set of pilot scale trials in wastewater treatment with a pneumatic distributor system for two banks of conventional aerators, called membrane diffusers, was the *decrease* in power consumption by the fluidic oscillator inserted as the splitter between the two banks (see Fig. 3). Typically, one expects that the insertion of a fitting into a flow distribution system, such as a bend, valve, or splitter will add an additional hydraulic resistance to the system. So the design trade-off for microbubble generation driven by a fluidic oscillator would be expected to be increased mass transfer performance scaling with the ratio of the diameter typical bubble generated by free stream steady flow and the microbubble diameter generated by fluidic oscillation, and the expected additional head loss at a constant volumetric flow rate. Clearly, the unexpected hydraulic resistance decrease of oscillatory flow requires an explanation. We believe there are two components to the decrease.

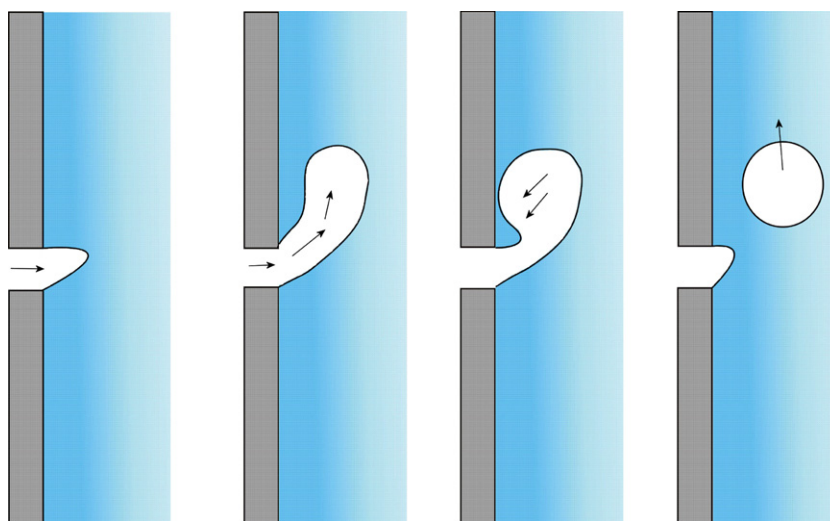


Fig. 6 – An schematic of the microbubble generation from a horizontally oriented nozzle/gas flow path. There are four distinct phases: (1) pushing out of a hemispherical cap at the beginning of the upstroke of the fluidic oscillator; (2) buoyant rise of the growing bubble during the remainder of the upstroke; (3) suction of the bubble to collide against the solid surface; (4) recoil of the bubble from the solid surface and breakoff of the bubble.

2.3.1. Coanda effect friction reduction

The fluidic oscillator in Fig. 3, on time average, serves as a splitter. The aggregate flow rate through each exit channel is equal, yet the flow never flows down both channels simultaneously. If the feedback loop were omitted, i.e. the control ports closed off (Fig. 2), then it would be expected that the fluid would fill the ducts on both sides due to the splitter action. This is exactly what happens in our control experiment, where the fluidic oscillator is replaced by tee-splitter. The tee-splitter and the closed-off control ports on the oscillator achieved almost exactly the same energy consumption at constant volumetric flow rate. In both cases, the splitter action results in the mean flow having a stagnation point at the geometric point of the split, regardless of the design of the splitter. Conversely, when the jet flows through either channel in the fluidic oscillator driven flow, the jet attaches to the curved sidewall in Fig. 1 according to the Coanda effect. Although this flow smoothly curves toward the outlet port, the diverted jet has no stagnation point. The friction loss along the wall at and near a stagnation point is appreciable, and is completely avoided by either diverted jet in a fluidic oscillator.

2.3.2. Boundary layer effects

Turbulent flow in ducts experiences a viscous sublayer near the wall in which dissipation is largest, exceeding the interior dissipation from eddy motions in the bulk. It is well known that solid bounding surfaces induce most of the dissipation loss in statistically stationary turbulent flows. But what about oscillatory flows with the same average volumetric flow rate? Since our oscillation is a “positive displacement” synthetic jet, it is conceptually useful to view it as a series of momentum pulses separated by momentum “gaps”. The fluid is suddenly accelerated by the momentum pulse, and then its inertia trails off until the next momentum pulse is excited. A conceptual model for this is the classical boundary layer problem of the suddenly accelerated plate, for which the frame of reference is changed to the stationary plate with the fluid suddenly accelerated. The laminar result is presented in the classical work by Rosenhead (1963). The thickness of the laminar boundary layer δ and the skin friction coefficient C_f are given, in dimensionless form, by

$$\frac{\delta}{x} = \frac{5}{\sqrt{Re_x}} \quad C_f = \frac{0.664}{\sqrt{Re_x}} \quad (6)$$

where x is the downstream coordinate from the start of the pulse. With a laminar boundary layer at high Reynolds number, one could argue that the time to set up the boundary layer should be inversely related to the dimensionless boundary layer thickness, and thus scaling with the square-root of the Reynolds number. So the time to set up a boundary layer is large. What if the period of the fluidic oscillator switches before the boundary layer is set up? That problem for dual laminar impinging jets has been studied by Hewakandamby (2008). The heat transfer coefficient for the oscillating impinging jet was found to be much higher than under steady dual impinging jets, as the oscillation disrupts the formation of the boundary layer that limits the transfer to the surface to conduction through the boundary layer. This principle works as well for mass and momentum transfer. The transfer rate to the impinging surface is much higher due to the disruption in setting up the boundary layer in the direction opposite of the impinging jets. Clearly, the argument

works as well for a single impinging jet. Tesař et al. (2007) show a similar conclusion experimentally for turbulent heat transfer.

The speculation here is that oscillatory flow reduces skin friction since the viscous boundary layer is disrupted in forming in the direction perpendicular to the flow. The momentum pulses find much less resistance in pushing down the center of the channel than from the slower moving fluid near the wall, as the viscous friction has not had time to “diffuse” outward from the sink of momentum at the wall.

This argument for skin friction reduction works as well for turbulent flow, but the time scales for turbulent wall boundary layer establishment are shorter in scaling factor, but given the much higher Reynolds number achievable in turbulent flow, this feature can be overcome with higher flowrates (or faster oscillation). The classical estimates for turbulent boundary thickness and skin friction are:

$$\frac{\delta}{x} = \frac{0.385}{Re_x^{1/2}} \quad C_f = \frac{0.0594}{Re_x^{1/2}} \quad (7)$$

Without any detailed experimental study, the results from our pilot trials suggest that these two resistance reduction effects – Coanda effect removing the stagnation point of the splitter and skin friction reduction by slow boundary layer formation – are estimated to be about equal in importance, about 6–7% reduction each with one volumetric flow rate, with the inference based on a roughly linear decrease in energy consumption with increasing oscillation frequency at high frequencies, but a plateau in reduction at low frequencies, but too little data for a more accurate assessment. Higher flow rates led to greater energy consumption savings, consistent with the implication of Eq. (2) and our assumption about the scaling of the time to set up a turbulent boundary layer.

3. Design aspects of an airlift loop bioreactor

In the previous section, the design aspects of a microbubble generator component of an airlift loop bioreactor were discussed, demonstrating that the usual design trade-off between friction losses with small apertures and distributor channels and performance gains in transfer efficiency with small bubbles can be “triangulated” with the fluidic oscillator principle, with the oscillatory flow resulting in less friction loss while still generating small bubbles. This argument poses the advantage of using such a fluidic oscillator driven microbubble generator in many chemical engineering processes, but still leaves many design questions. Before a design can be confidently implemented, information must be collected on performance aspects that are affected by inclusion of the novel element in the design. In this section, we will address the likely influence of the microbubble generator on the typical performance of an ALB. However, this is recognized as no substitute for actual performance observation and results of operational studies. There is a “chicken-and-the-egg” problem here that in order to design an ALB properly with this novel component, it is necessary to construct, commission and operate a prototype. But the prototype must be designed. The scope of this article is the design of the prototype, whose operational performance variation can then be reported on in due course.

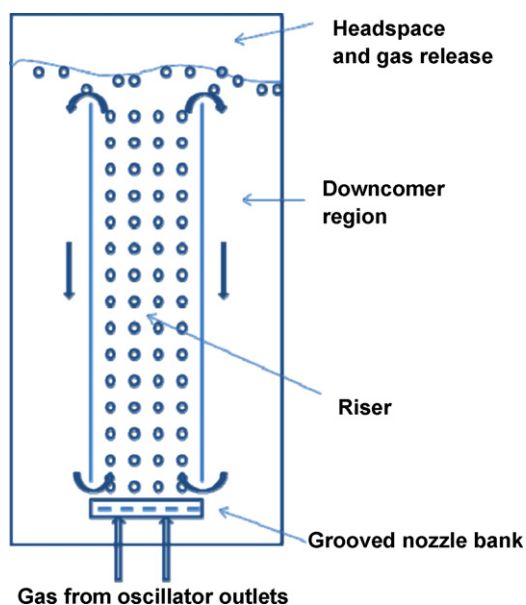


Fig. 7 – Schematic diagram of an internal ALB with draught tube configured with a tailor made grooved nozzle bank fed from the two outlets of the fluidic oscillator. The microbubble generator is expected to achieve nearly monodisperse, uniformly spaced, non-coalescent small bubbles of the scale of the drilled apertures.

3.1. Key design features of an ALB

In this subsection, we will review key design features of the ALB with a view to the influence of the microbubble generation mechanism. A fuller review is given by Jones (2007).

Fig. 7 shows the schematic diagram of the internal draught tube ALB configured with a tailor-made grooved nozzle bank such as demonstrated in Fig. 4. This is expected to achieve nearly monodisperse, uniformly spaced, non-coalescent small bubbles of the scale of the drilled apertures. The cloud of dispersed microbubbles should resemble Fig. 5. This is the major modification of the ALB proposed here. The remaining features of the internal draught tube, riser, and downcomer regions are conceptually the same as the standard design, which drives the recirculating flow from buoyant effects – a combined forced and free convection flow, as there is an injection of momentum, but also of density difference. The bubbly flow region has lower density, and rises due to a combination of buoyant and hydrodynamic forces (Grammatika and Zimmerman, 1999, 2001). The downcomer flow is assured by the kinematics – if fluid rises in the riser, then the bottom of the riser is a mass sink and the top is a mass source due to continuity. Consequently, this drives a flow from the top of the riser to the bottom, shown by the arrows in Fig. 7.

3.1.1. ALB base

Merchuk and Gluz (1999) have the most promising work on the ALB base area, but until their contribution, it would be fair to state that most researchers have viewed the base as of little consequence to ALB performance. As the gas sparger and the bubble distribution are located in the base, this is the major focus of our design, as can be seen in Fig. 7, where our fluidic oscillator and tailored grooved nozzle bank distribution system has been substituted for the traditional base. The only hydrodynamic issue otherwise about the base how the liquid from the downcomer region is drawn in through the base

to the riser region. Sufficient clear space for this drawing in should be available so that friction losses are not appreciable. As the free and forced convection flow in Fig. 7 has only a finite amount of kinetic energy available, as supplied by the injection flow and contributed by the dragging of the liquid by the rising bubbles, friction losses should be minimised everywhere, as the flow is holistic throughout the ALB – changes in one section are propagated throughout. In this respect, the oscillatory flow which was responsible for lower friction in the pipework of the wastewater treatment experiment mentioned in Section 2.3 may contribute within the ALB as well to lower friction losses. In the underwater visualizations of microbubble cloud formation, a concerted, periodic motion of toroidal shaped clouds of bubbles were observed, indicating that the oscillatory effect can extend beyond the microbubble generation in the base. These toroidal clouds were observed at relatively low frequencies, 1–5 Hz, i.e. long feedback loops ~25 m.

3.1.2. ALB riser

The riser is the phase transfer work-horse of the ALB. The gas–liquid mass transfer and liquid–bioculture mass transfer are the dominant features of this region. The gas sparger is usually at the bottom of the riser, and the bubbly flow is responsible for the lowest density in the fluid mixture, and for the co-current flotation effect in the ALB. This section is the major target for performance enhancement for the introduction of microbubbles. If nutrients are introduced in the gas phase, such as oxygen for aerobic metabolism, the higher mass transfer flux should lead to greater bioculture activity, or conversely, low gas flow rates could be introduced to save energy consumption while achieving the same oxygen transfer rate, due to the higher oxygen transfer efficiency as discussed in Section 2.1. According to the hydrodynamic bubble chain stabilization hypothesis by Crabtree and Bridgwater (1969), we expect, as in Fig. 5 and illustrated in Fig. 7, that the microbubbles generate will be nearly monodisperse and uniformly spaced as they rise. This should significantly change the multiphase flow dynamics with more uniform profiles and predictable mass transfer coefficients. It is the deformability and polydispersity of bubble clouds that makes mass transfer and momentum transfer effects from gas to liquid phase reliant on empirical correlations. With uniformly spaced, monodisperse bubbles, the mass transfer coefficient can be predicted from level set method modelling such as those of Deshpande and Zimmerman (2005a,b), and the hydrodynamic effects by the concerted multibody microhydrodynamics analysis of Grammatika and Zimmerman (2001). The generalized flotation analysis of this paper is particularly important as the introduction of smaller bubbles in the riser region can lead to a much greater flotation effect from the collection, by microbes, of sufficient microbubbles on their surfaces to have an appreciably larger flotation efficiency, such as the major feature of dissolved air flotation separations. The tailoring of the microbubble scale to achieve the desired level of fluidization of the bioculture without collecting the whole of the phase at the gas–liquid interface at the head space is a major design problem for this novel ALB. Performance data at the moment is required, as previous studies on the effect of changing the geometric parameters of the perforated plate distributor system have largely been about the uncovered area of the plate, not the size distribution of the bubble clouds generated.

Typically gas–liquid multiphase flow may have a wide range of regimes, but dispersed or bubbly flow is common in all

applications. These possible flow regimes are dependent on the geometrical configuration and the gas and liquid superficial volumetric flow rates. The influence on flow regime of the microbubble generation system is not known *a priori*. Nevertheless, it would seem highly likely that it will have a strong influence, for instance, the toroidal mode of bubble cloud formation observed in air diffuser trials discussed before have no analogue in the standard pipeline flow regimes as the bubbles are practically monodisperse and non-coalescent, yet otherwise expected to be in the heterogeneous flow regime. Clearly, the observed flow regimes will depend on the liquid viscosity for low loading of microbes, and on the effective rheology of the suspension when there is a large volume fraction of microbes. The robustness of the flow diagram in Fig. 7 must be tested experimentally, particularly with regard to entrainment in the downcomer region and channelling in the riser.

The performance of an ALB is likely to be affected by the modification of the flow regimes, as the biological growth has been shown to be sensitive to flow regime (Vial et al., 2000). Our own biological growth studies focussed on the yield of yeast biomass from microbubble generation with fluidic oscillation, which was shown to be 15% higher than growth under steady flow (Zhang, 2007). However, we limited our growth study to the bubbly homogeneous flow under low flow rate conditions, where the higher growth rate could be attributed to higher dissolved oxygen levels from higher mass transfer coefficients, not the flow regime itself.

3.1.3. ALB downcomer

This is probably the least dynamically important region of the ALB, as the downcomer flow is determined by kinematic considerations, and its composition and bioculture occupation are dependent on the particulars of the riser design. This region has the highest multiphase density, largely occupied with liquid, perhaps with high dissolved oxygen (gas) concentration, but the gas phase hold up is expected to be large only if microbubbles are small enough to be entrained in the liquid flow as passive scalars. Such entrainment is unlikely, for instance, with purely free convection driven flow, as none of the bubbles should be sufficiently large to disrupt the orderly flow as depicted in Fig. 7. However, if there is a strong forced convection component, it is possible that the bubble rise will sufficiently transfer momentum to the liquid that the liquid phase flow will be strong enough to entrain some of the microbubbles in the downcomer. Clearly, this aspect of the novel ALB design posed here is much different than in conventional ALBs.

3.1.4. Gas separator

The region at the top of the riser to the top of the downcomer is termed the gas separator. It is not our intention to change anything in the design of this sensitive area, but it is commonly accepted that this is the most sensitive part of the ALB design. Residence time of fluid in the gas separator depends globally on the design and on the conditions, particular gas holdup, in the riser and downcomer. Merchuk and Siegel (1988) discusses many of the key aspects of gas separator design.

3.2. Flow circuit design and instrumentation

In the equipment design, the process flow into the bioreactor has been considered carefully for tight control of the temperature and air flow. This is deemed necessary for the comparison of the performance with and without oscillations. The tem-

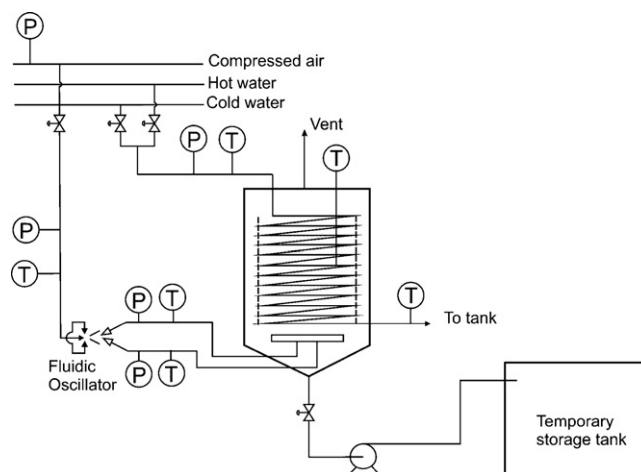


Fig. 8 – Process flow diagram of the airlift bioreactor gas separator.

perature control is to be achieved through a cooling fluid, preferably water, and utilization of a copper coil. The coil is placed inside the bioreactor to support the internal baffle that acts as the flow guide. The temperature and the pressure/flow rate of the coolant are to be monitored continuously to control the flow. A thermocouple is placed inside the bioreactor as the control probe that regulates the coolant control valve using an external controller (LabView PCI control card). The flow in the temperature regulation circuit is designed to switch between hot and cold coolant streams, adding the flexibility to use the same circuit to heat the system if necessary (Fig. 8).

The compressed air stream comes from a constant head compressor is connected to the diffuser through a fluidic oscillator that can be tuned to adjust the oscillation frequency in the range of 1–100 Hz. The novelty in the process is the inclusion of the oscillator to generate smaller bubbles. As a comparison of aeration levels between oscillated and the steady air flow has to be made, the control and the measurements of the air flow circuit is crucial to the experiments. Both the pressure and the temperature are to be measured upstream and downstream from the fluidic oscillator. The oscillator has the nozzle effect that expands the flow and the temperature change and the pressure loss across it has to be considered carefully in the comparison. This means that a slightly higher pressure has to be employed when the oscillator is in place as the time averaged pressure head to the diffuser should be same for both cases. To this end, a pressure regulator is used between the mains and the oscillator. Temperature of the compressed air, which is difficult to control, is to be measured prior to the diffuser and the surface tension and the volume expansion/contraction are to be compensated in the calculation.

The bioreactor discharges its load to a holdup tank at the base level for further processing. A centrifugal or a positive displacement pump is to be used to pump the slurry to the tank depending on the thickness. For thin slurry, the gravity flow would be sufficient.

3.3. Bioreactor design

The capacity of the tank is 250 l and an excess of 10% is provided as a safety measure to prevent spills. It consists of a conical bottom with an angle of 75° a cylindrical section and a bolted end plate with a vent. If the anaerobic conditions are to be maintained the flow through the vent could be

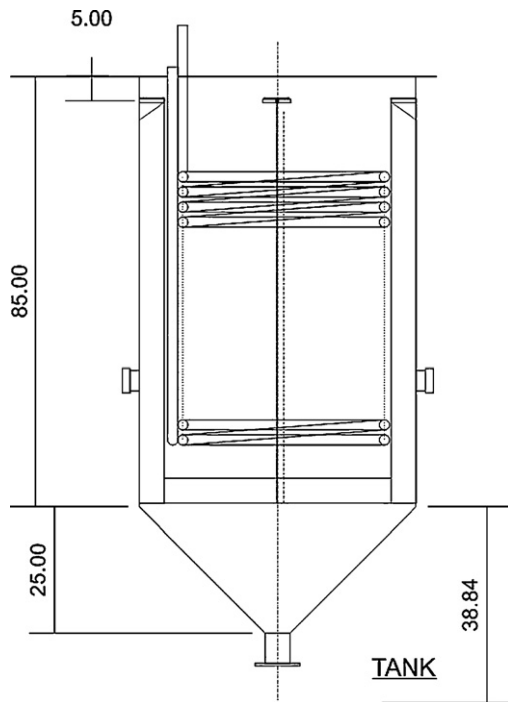


Fig. 9 – The design of the bioreactor (dimensions are centimeters).

regulated using a valve. 2 mm stainless steel (SS 405 general purpose) is used to fabricate the vessel. Two optical ports are provided for imaging and observation with fitted borosilicate glass.

The baffles are fitted into the bioreactor with a nut and bolt mechanism with support guides. These can be dismantled for cleaning purposes. The baffle attachments also support the diffuser plate. The rationale is to allow complete dismantling of the parts to clean between different batches where the microorganisms in action are of different types. The temperature is controlled by pumping a coolant through a copper coil that encompasses a circular area of diameter of 0.55 m. Copper tubing with 1 cm OD is used to fabricate the coil. The pitch of the coil is 1.8 cm. The coil is self-supported and fixed to the top endplate. A cylindrical baffle made of Perspex (to enable optical access) goes around the coil. This baffle is fitted to the top endplate. A rubber gasket between the vessel flange and the endplate provide an airtight seal. Fig. 9 shows the assembled bioreactor.

3.4. Diffuser flow distribution

The design of the channel arrangement follows the rationale given in Section 2.2.2. The design requires placing an optimum number of nozzles in one manifold without hindering the formation of monodispersed bubble arrays. The minimum distance between two nozzles should be greater than one bubble diameter in order to prevent coalescence of bubbles to form bigger bubbles. Larger distances minimise the lift leading to poor internal circulation. To design a bubble swarm, that does not affect the transportation of relevant gasses, providing maximum lift is an experimental process that will be undertaken as the part of the proposed experiments. However, as a starting point, the nozzles are placed two nozzle diameters apart along the manifold axis.

Each manifold is connected to a common distributor. The distributor is connected to the compressed air main supply

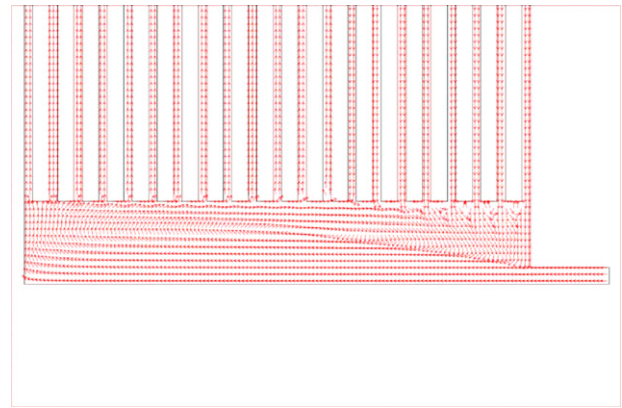


Fig. 10 – Flow field within the distributor when a pressure gradient of 10 Pa applied across it. A negative pressure develops near the inlet.

(with or without the oscillator depending on the configuration). The position of the inlet port and the distributor geometry affects the flow distribution to the nozzle manifolds. The distribution patterns are examined before the design stage using CFD. The 2D study using simple $k-\epsilon$ turbulent flow model with varying inlet position is carried out. The size of the diffuser plate and the possible channel/chamber geometries are limited by the tank dimensions as well as fabrication techniques available to us at the moment. With these restrictions the best possible distribution is to be achieved using CFD as a design tool. Fig. 10 shows the maldistribution of air to the manifolds when the inlet port is placed on the side of the distributor. Fig. 11 shows the average pressure within the nozzle manifolds for two pressure drops; 1 Pa and 10 Pa across the diffuser. Pressure within the channels closer to the inlet become increasingly negative as the pressure drop increases. This has an adverse effect as the flow in the nozzle manifolds inverts. This indicates the possibility of flooding of the distributor leading to operational problems. Modifications to the distributor geometry have minimised the maldistribution. Fig. 12 shows a different geometry and the flow induced by applying 10 Pa pressure drop across the diffuser. Fig. 13 shows the pressure distribution in the nozzle manifolds. This geometry guarantees a positive pressure head in all channels eliminating the possibility of flooding of the diffuser.

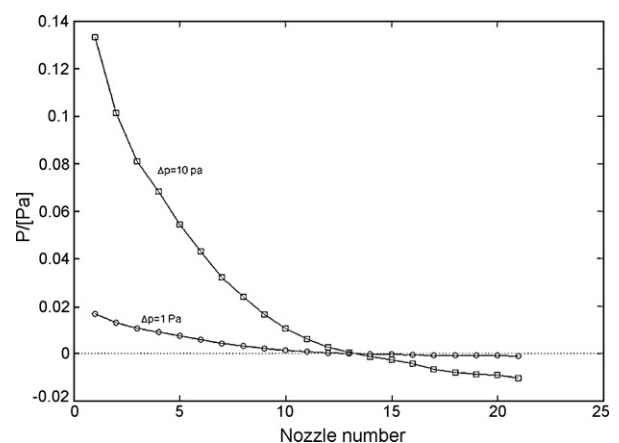


Fig. 11 – Pressure distribution in the nozzle manifolds. Nozzle count is from left to right (of the arrangement shown in Fig. 10). The negative pressure is due to the nozzle effect at the inlet area.

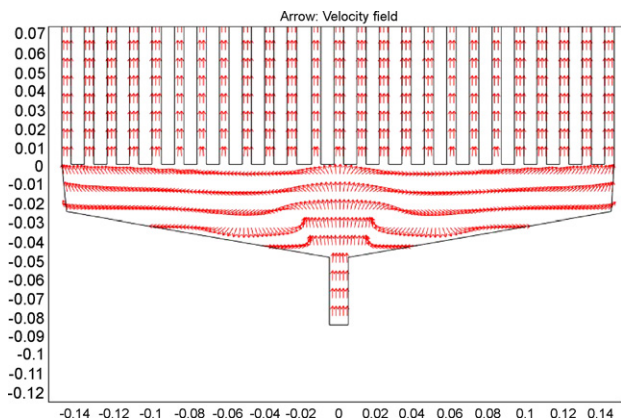


Fig. 12 – Flow field within the distributor when the inlet is place at the centre parallel to the nozzle manifolds. Pressure gradient across the distributor is 10 Pa.

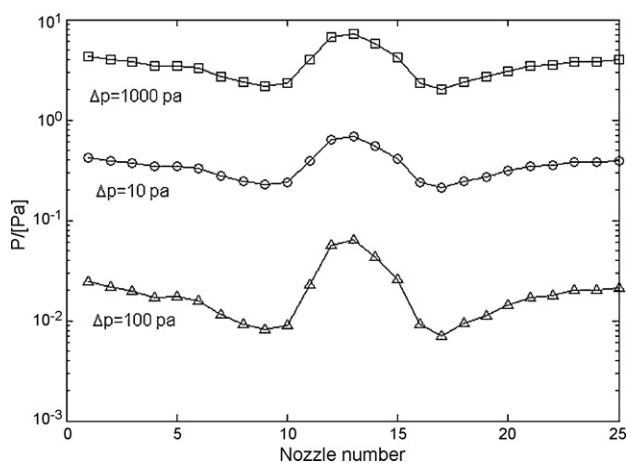


Fig. 13 – Pressure distribution in the nozzle manifolds for the geometry shown in Fig. 12. Nozzle count is from left to right.

4. Discussion and conclusions

This paper presents the many advantages of a microbubble generation mechanism actuated by fluidic oscillation – potential low energy consumption, high heat, mass, and momentum transfer rates, flotation and flocculation potential – and argued for its inclusion in a standard design of a draught tube internal loop airlift bioreactor. The expected impact on the canonical design for such an ALB is discussed, particularly with regard to the expected nearly monodisperse, non-coalescent bubbly flow regime that should be maintained to high gas flow rates. These qualitative features are combined into the altered ALB design presented in Section 3, for which the dynamics are simulated and the design is collated. The design of the nozzle bank of the distributor was optimized using CFD to achieve best uniformity of flow. Future works will assess the operational performance of this design, particularly with a view towards operating guidelines and design knowledge.

Acknowledgements

WZ would like to thank support from the EPSRC for the development of the acoustic actuated fluidic oscillator (Grant No. GR/S67845) and for financial support from the Food Processing Faraday Partnership, Yorkshire Water, Sheffield University

Enterprises Ltd., the European Union Objective 1 Fund administered through the University of Sheffield, and Wastetoethanol Ltd. WZ would like to thank the Royal Academy of Engineering/Leverhulme Trust Senior Research Fellow programme. The authors wish to acknowledge the support of Simon Butler and the assistance of Hu Shi, Amar Varma, Shu-Chen Kuo, and Xingyan Zhang, as well as helpful discussions with Eddie Todd (Wastetoethanol Ltd) and Ted Heindel. VT acknowledges the financial support obtained through the research project AV0Z20760514 at the Institute of Thermodynamics of the Academy of Sciences of the Czech Republic. Technical support from Adrian Lumby, Clifton Wray, Mark O'Meara, Andy Patrick, and Oz McFarlane is much appreciated.

References

- Bredwell, M.D. and Worden, R.M., 1998, Mass-transfer properties of microbubbles. 1: Experimental studies. *Biotechnology Progress*, 14(1): 31–38.
- Chisti, M.Y. and Moo-Young, M., 1987, Airlift reactors: Characteristics, applications, and design considerations. *Chemical Engineering Communications*, 60: 195–242.
- Crabtree, J.R. and Bridgwater, J., 1969, Chain bubbling in viscous liquids. *Chemical Engineering Science*, 24: 1755–1768.
- Deshpande, K.B. and Zimmerman, W.B., 2005, Experimental study of mass transfer limited reaction. Part I: A novel approach to infer asymmetric mass transfer coefficients. *Chemical Engineering Science*, 60(11): 2879–2893.
- Deshpande, K.B. and Zimmerman, W.B., 2005, Experimental study of mass transfer limited reaction. Part II: Existence of crossover phenomenon. *Chemical Engineering Science*, 60(15): 4147–4156.
- Grammatika, M. and Zimmerman, W.B., 1999, Neural network modelling of surface aeration in fermenters. *Mixing VI. IChemE Symposium Series*, 146: 227–234.
- Grammatika, M. and Zimmerman, W.B., 2001, Microhydrodynamics of flotation processes in the sea surface layer. *Dynamics of Oceans and Atmospheres*, 34: 327–348.
- Heijnen, J.J. and Van't Tiet, K., 1984, Mass transfer, mixing and heat transfer phenomena in low viscosity bubble column reactors. *Chemical Engineering Journal and the Biochemical Engineering Journal*, 28(2): 21–42.
- Hewakandamby, B.N., 2008, A numerical study of heat transfer performance of oscillatory impinging jets. *Journal of Heat & Mass Transfer*, doi:10.1016/j.jheatmasstransfer.2008.07.004
- Jones, S.T., 2007, Gas–Liquid Mass Transfer in an External Airlift Loop Reactor for Syngas Fermentation, Ph.D. Dissertation, Department of Mechanical Engineering, Iowa State University, Ames, Iowa.
- Merchuk, J.C. and Gluz, G., 1999, Bioreactions, air-lift reactors, in *Bioprocess Technology: Fermentation, Biocatalysis, and Bioseparation*, Flickinger, M.C. and Drew, S.W., Drew, S.W. (eds) (John Wiley & Sons), pp. 320–352.
- Merchuk, J.C. and Siegel, M.H., 1988, Airlift reactors in chemical and biological technology. *Journal of Chemical Technology and Biotechnology*, 41: 105–120.
- Rosenhead, L., (1963). *Laminar Boundary Layers*. (Clarendon Press, Oxford).
- Shi, H., 2006, Novel Bubble Aerator Performance, University of Sheffield, MSc in Environmental and Energy Engineering dissertation.
- Stevenson, D.G., (1997). *Water Treatment Unit Processes*. (Imperial College Press, London).
- Tesař, V., (2007). *Pressure Driven Microfluidics*. (Artech House, Boston).
- Tesař, V., Hung, C.-H. and Zimmerman, W.B., 2006, No moving part hybrid synthetic jet mixer. *Sensors and Actuators A*, 125(2): 159–169.
- Tesař, V., Travnicek, Z., Kordik, J. and Randa, Z., 2007, Experimental investigation of a fluidic actuator generating

- hybrid-synthetic jets. *Sensors and Actuators A*, 138(1): 213–220.
- Varma, A., 2007. *Microbubble Generation for the Enhanced Air Lift Recovery of Oil From Oil Sands*, University of Sheffield, MSc in Environmental and Energy Engineering dissertation.
- Vial, C., Cmarassa, E., Poncin, S., Wild, G., Midoux, N. and Bouillard, J., 2000, Study of hydrodynamic behaviour in bubble columns and external loop airlift reactors through analysis of pressure fluctuations. *Chemical Engineering Science*, 55: 2957–2973.
- Worden, R.M. and Bredwell, M.D., 1998, Mass-transfer properties of microbubbles. 2: Analysis using a dynamic model. *Biotechnology Progress*, 14(1): 39–46.
- Zhang, X., 2007, *Novel aerator studies on yeast growth*, University of Sheffield, MSc in Environmental and Energy Engineering dissertation.
- Zimmerman, W.B. and Homsy, G.M., 1991, Nonlinear viscous fingering in miscible displacement with anisotropic dispersion. *Physics of Fluids A*, 3(8): 1859.
- Zimmerman, W.B.J. (ed), 2005a, *Microfluidics: History, Theory, and Applications* (Springer-Verlag–Wien, Berlin), CISM Lecture Series, No 466, 300 pp.
- Zimmerman, W.B., Tesař, V., Butler, S.L. and Bandulasena, H.C.H., 2008, Microbubble generation. *Recent Patents in Engineering*, 2: 1–8.